processes

MDPI

Article

Fatigue Crack Propagation Behavior and Life Prediction of Welded Joints of SMA490BW Steel for Bogies

Xingyuan Xu [1], Liyang Xie [1], Song Zhou [2,*], Jinlan An [2], Yanqing Huang [2] and Dongxia Li [3]

[1] School of Mechanical Engineering and Automation, Northeastern University, Shenyang 110004, China
[2] Key Laboratory of Fundamental Science for National Defense of Aeronautical Digital Manufacturing Process, Shenyang Aerospace University, Shenyang 110136, China
[3] School of Mechanical and Electrical Engineering, Shenyang Aerospace University, Shenyang 110006, China
* Correspondence: zhousong23@163.com

Abstract: In this paper, the precrack propagation behavior of an SMA490BW welded joint in the core zone and heat-affected zone was analyzed through experiments based on the FRANC 3D and ABAQUS cosimulation method, and life prediction of these cracks was also investigated. The results show that the experimental crack propagation path and crack propagation rate in the weld core zone and heat-affected zone agree well with the simulation results, with a small relative error. The life span of the prefabricated crack in the heat-affected zone was higher than that in the core zone. Furthermore, regarding the life prediction results for the two samples, the relative error obtained using FRANC 3D was about 5%, which was verified using the method of joint simulation of crack propagation behavior in the zone simulation and their life prediction with accurate feasibility.

Keywords: SMA490BW; FRANC 3D; crack propagation; life prediction

Citation: Xu, X.; Xie, L.; Zhou, S.; An, J.; Huang, Y.; Li, D. Fatigue Crack Propagation Behavior and Life Prediction of Welded Joints of SMA490BW Steel for Bogies. *Processes* **2023**, *11*, 1984. https://doi.org/10.3390/pr11071984

Academic Editor: Prashant K. Sarswat

Received: 2 June 2023
Revised: 25 June 2023
Accepted: 27 June 2023
Published: 30 June 2023

1. Introduction

Today, the world's high-speed rail industry aims to realize higher speed, smoother operation, lighter weight, and better network connectivity. As a core component of a high-speed train, bogies have a complex structure and play a decisive role in the stability and safety of train operation [1–3]. Welding is a key connection mode in bogie manufacturing, and fatigue failure is the main failure mode of welded joints. In practical engineering applications, cracks will inevitably appear when mechanical structures operate in complex environments. Moreover, most of the fatigue failures of mechanical structures are caused by initial cracks that continuously expand forward under the action of alternating loads, thereby causing great losses to people's lives and safety. Therefore, it is particularly necessary to study the fatigue crack propagation behavior of welded joints of high-speed train bogies.

SMA490BW is widely used in the manufacture of high-speed train bogies due to its exceptional mechanical properties and toughness. Therefore, research on the performance of SMA490BW welded joints has attracted extensive attention from scholars at home and abroad. Wu et al. [4] conducted a mechanical property test to study the microstructure of the flat butt joint of SMA490BW steel welded via manual, single-wire automatic, and double-wire automatic welding. They found that the strength and impact toughness of the joint welded using the above methods meet the design requirements, with the double-wire welding showing excellent advantages, such as energy savings and improved welding productivity. Xu Liang et al. [5] studied the fatigue properties of SMA490BW in different sampling directions and stress ratios. The results show that the ultimate fatigue stress of samples in the T-L (along the rolling direction) sampling direction was 5.4% higher than that in the L-T (vertical rolling direction) direction. Under the same maximum cyclic stress, the fatigue strength increased with an increase in the stress ratio R. He et al. [6] studied the influence of ultrasonic impact treatment on the ultra-high-cycle fatigue properties of an

SMA490BW welded joint. They found that the high-cycle or even ultra-high-cycle fatigue properties of welded joints were significantly improved after ultrasonic impact treatment. Simultaneously, the grain refinement and work-hardening effects after ultrasonic treatment led to an increase in surface microhardness. Wu et al. [7] studied the corrosion behavior of SMA490BW used for high-speed train bogies and its welded joints using a periodic wet/dry cycle corrosion test simulating an industrial atmospheric environment. The results show that the corrosion weight loss rate decreased with an increase in the corrosion time. The corrosion loss rate of the welded joint was lower, and its corrosion resistance was better than that of the SMA490BW steel under simulated industrial atmosphere. Some scholars have studied the crack propagation behavior of SMA490BW welded joints. Zhang et al. [8] took SMA490BW welded joints as a research object to study the influence of various humidities (50%, 60%, 70%, 80%, and 90%) on the crack propagation of welded joints. They found that humidity had little effect on the crack propagation rate through microstructure observation. Li Ning et al. [9] established a finite element model using ABAQUS and calculated the fatigue performance of a 12 mm thick SMA490BW butt joint crack propagation sample by comparing it with the BS7910 standard [10]. The results show that the two-stage crack propagation model can accurately predict the fatigue life of butt joint cracks, and the model results are highly consistent with the test results.

Additionally, finite element software is being increasingly used in crack propagation research with the advancements in computer technology. As a fracture mechanics analysis software, FRANC 3D can be used to analyze the direction of crack propagation more accurately and significantly improve the accuracy and efficiency of the model. Therefore, its usage along with other finite element software for three-dimensional fatigue crack simulation analysis is gradually becoming a hot research topic. Xiong Xun et al. [11] analyzed the crack propagation behavior of CT specimens of Q235 steel based on the cosimulation of FRANC 3D and ABAQUS. They confirmed the accuracy and rationality of the cosimulation through the test results. Liao [12] and Park et al. [13] conducted simulation analysis on the crack propagation of complex geometry using the FRANC 3D software (7.5.6) and verified the reliability of the simulation results through test results and theoretical calculations. Giannella et al. [14,15] studied the fatigue crack propagation behavior of a railway shaft through FRANC 3D, and evaluated the crack propagation rate, providing a feasible method for making maintenance plans according to the damage tolerance principle.

In summary, scholars are mostly focused on studying the microstructure, mechanical properties, and fatigue properties of SMA490BW welded joints at present. However, there is a lack of research on its crack propagation behavior, even though there are a few reports on crack propagation behavior analysis in the welding area. Therefore, it is impossible to accurately evaluate and predict the life span of cracked welded structures. In this paper, an SMA490BW welded joint was used as the research object to compare the results of FRANC 3D and ABAQUS cosimulation, for the in-depth study and analysis of the crack expansion behavior in different areas of the welded joint, and then life prediction and a detailed analysis of fracture topography were carried out to provide a basis for bogie fatigue design and safety evaluation.

2. Experimental Method and Finite Element Simulation

2.1. Experimental Materials

The test material was SMA490BW, a low-alloy high-strength weathering steel imported from Japan. SMA490BW steel contains elements such as P, Ni, Cu, and Cr, which are resistant to atmospheric corrosion. These elements will produce a protective film of air isolation on the steel surface after the corrosion of the steel, preventing the material from remaining in contact with the air and causing corrosion. Thus, the corrosion performance of the sample is improved, and its chemical composition is shown in Table 1. In this experiment, MAG fusion welding was used for the butt welding of SMA490BW. Further,

a CHW55-CNH welding wire with a diameter of 1.6 mm and 80% Ar + 20% CO_2 as a protective gas were used for welding.

Table 1. Chemical composition of SMA490BW steel (wt%) [16].

C	Si	Mn	P	S	Cu	Ni	Cr
≤0.18	0.15~0.65	≤1.40	≤0.035	≤0.006	0.30~0.50	0.05~0.30	0.45~0.75

For the fatigue crack propagation test, a central crack tensile sample (MT) was used. The sample's dimensions were 250 mm × 60 mm × 3 mm. Figure 1 shows the specific size of the sample. The cracks were prefabricated in the core zone (NZ) and the heat-affected zone (HAZ).

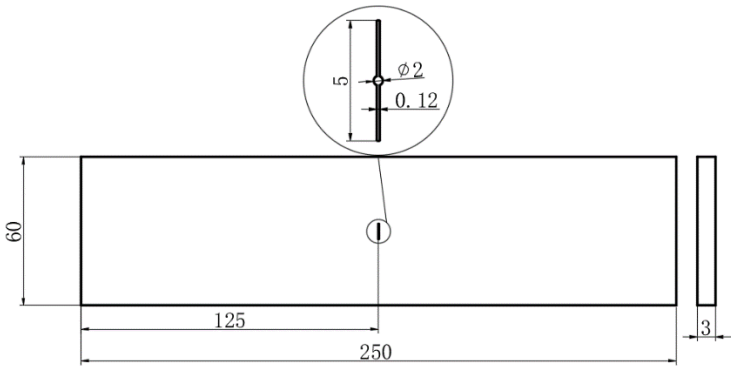

Figure 1. Specimen of fatigue crack propagation rate.

2.2. Experiment Content

The fatigue crack propagation test was performed on the MTS810 fatigue test machine at room temperature. The test was conducted with the sinusoidal loading mode of R = 0 and F = 30 kN, and the test frequency was selected as 20 Hz. Before the experiment, the test piece was polished with 240–2000-grit sandpaper until it was bright; then, it was polished with a diamond polishing agent, and finally corroded with a mixture of 4% nitric acid–96% methanol (volume fraction). Before the test, a gap of about 2 mm was prefabricated via wire cutting, and a special microscope with CCD was used to observe the changes in crack length. In the test, the prefabricated crack length was set to 1.5 mm in order to eliminate the influence of wire cutting on crack growth.

2.3. Finite Element Simulation

The fatigue crack propagation process was analyzed based on the ABAQUS and FRANC 3D cosimulation method. Because the mechanical properties of the joint materials were not uniform, their yield strength in each area of the joint was different, and the finite element model was processed in zones. The fatigue crack propagation process was analyzed based on the ABAQUS and FRANC 3D cosimulation method. The cosimulation method was mainly used to establish the model in ABAQUS. Because the mechanical properties of the joint materials were not uniform, the yield strength of the materials in each area of the joint was different, so the finite element model was processed in zones and the load was defined. FRANC 3D was mainly analyzed and derived in the process of crack growth, the length of the crack, the crack propagation rate, and the crack propagation life. In order to obtain the basic mechanical properties of SMA490 steel, it is necessary to carry out tensile tests. The sample was prepared in accordance with GB/T2975 [17] requirements, and the static tensile test was conducted in accordance with GB/T228.1-2010 [18]. The elastic modulus, Poisson's ratio, and material yield strength of SMA490BW welded joints in various regions, as obtained through preliminary tests, are shown in Table 2.

Table 2. ABAQUS input material parameters for different regions of welded joints.

	E/MPa	μ	σ_s/MPa
base metal	206,000	0.30	365
HAZ	206,000	0.26	398
NZ	215,000	0.35	369

As shown in Figure 2, the MT model divides each region in ABAQUS and assigns corresponding material properties to each region. The material parameters were obtained through an experiment. The relevant load and boundary conditions were defined. Either the left or right surface of the sample was selected to be defined as the coupling constraint relationship, and the other surface was defined as the cyclic load in the direction of Y. The load form was sine wave, and the maximum force of the applied load was 30 kN. During the finite element mesh division in ABAQUS, the mesh type of the 8-node quadrilateral planar strain CPE8 element was selected. Because the element type had the characteristics of high elasticity and strong plasticity, the mesh of the crack tip needed to be refined during the mesh division. We imported the inp. file in ABAQUS into FRANC 3D. In FRANC 3D, we set the prefabricated initial crack as an elliptic crack in size, and the elliptical crack was inserted at the wire cutting position, corresponding to the prefabricated crack of about 1.5 mm to eliminate the influence of wire cutting on crack propagation, and the length of the crack propagation direction was a = 1.5 mm. The length b = 5 mm in the thickness direction and the geometric radius of the crack tip unit were set to 0.05 mm to facilitate more accurate crack propagation simulation.

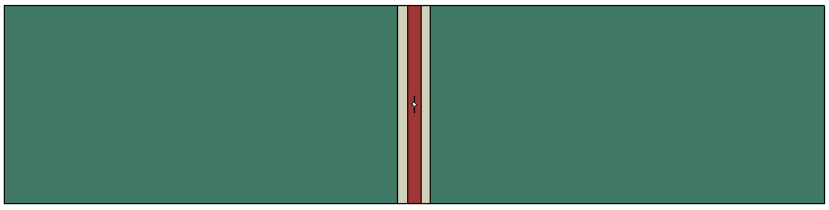

(**a**) NZ sample

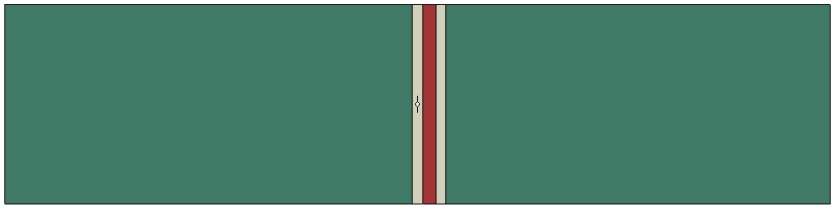

(**b**) HAZ sample

Figure 2. CT sample diagram of model partition (red—NZ; yellow—HAZ; green—base material area).

In online elastic fracture mechanics, the classical Paris formula [19,20] is the most widely used in engineering. Table 3 presents the basic parameters—C, m, and threshold values ΔK_{th}—of the prefabricated crack propagation in the NZ and HAZ in the multizone crack propagation test of the SMA490BW welded joint. The test process of the threshold value ΔK_{th} was carried out according to the test method specified in the national standard GB/T6398-2000 [21]. The test was carried out on an MTS 810 fatigue test machine using the K reduction method. The loading waveform was sine wave, the frequency was 20 Hz, and the test conditions were room temperature and air environment.

Table 3. Fatigue crack propagation basic Paris parameters.

Crack Location	m	C	ΔK_{th} (Mpa/m$^{1/2}$)
NZ	3.37	1.15×10^{-13}	5.939
HAZ	3.05	1.95×10^{-13}	4.895

3. Results and Discussion

3.1. Fatigue Crack Propagation Path

Figure 3 shows the crack propagation path of the SMA490BW welded joint containing precracks in the NZ and HAZ. The prefabricated cracks were in the NZ and HAZ samples, and the initiation, propagation, and transient fracture processes of the cracks were all in the weld zone. The cracks expanded along a straight line, but a small angle of deflection was observed in the transient fracture zone. The main reason for this is that the strength of the base material zone of SMA490BW is higher than that of the weld zone. In the final fracture zone, due to the rapid fracture of the crack, the driving force exerted causes the deflection of the crack. Figure 4a shows the crack propagation path of the NZ sample. During the test, the prefabricated crack stage was found, and the crack propagation path was straight and relatively smooth, and this continued until the stable stage of crack propagation was reached. The path of crack propagation fluctuates when it enters the phase of crack propagation instability. When the specimen crack extends far enough into the remaining force area, instantaneous fracture occurs. At this time, deflection of the crack was found in the transient fracture region of the NZ specimen, but this cannot be explained by the fatigue mechanism under a cyclic load, which can also be attributed to the plastic instability of the material and the failure of the specimen. Figure 4b shows the crack propagation path of the HAZ sample. During the test, it was found that the prefabricated crack propagation path of the HAZ sample was not smooth compared with that of the NZ sample. It was found that one side of the sample was deflected in the stable expansion stage, and the mechanical properties of the material in this part of the heat-affected region were not uniform. In the transient fracture region, compared with the crack propagation path of the NZ sample, the deflection occurred at the position with a longer crack length, and the crack failed directly instead of making a straight line after deflection.

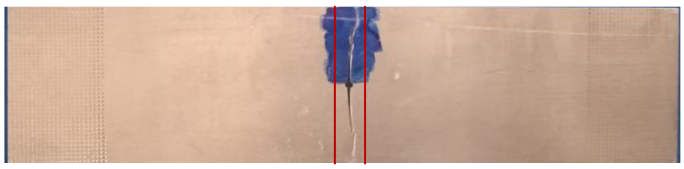

(**a**) NZ sample

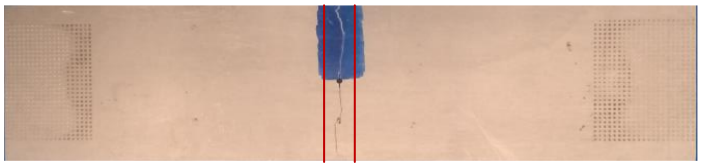

(**b**) HAZ sample

Figure 3. Multi-region crack propagation path of SMA490BW welded joint (Inside the red line is the weld area).

Figure 4 shows the crack propagation path of the HAZ and NZ areas obtained using FRANC 3D simulation. The crack propagation path of the two samples showed linear expansion. Compared with the test results, the simulation path did not show a small angle of deflection, because the simulation model cannot simulate the nonuniform distribution of the internal organization of the specimen. At the same time, it is difficult to deduce the transient broken region with the formula at present, and FRANC 3D simulation of the transient broken region needs further research, but in using FRANC 3D to simulate the crack propagation path, it was found that in the stable crack propagation stage, the simulation and test results are basically consistent.

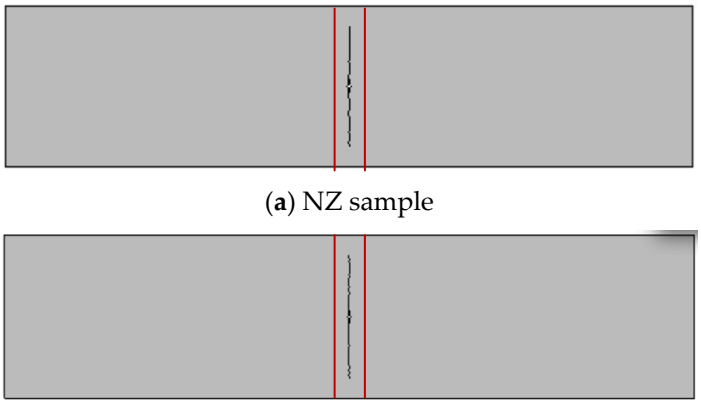

(**a**) NZ sample

(**b**) HAZ sample

Figure 4. FRANC 3D simulation of SMA490BW welded joint multi-region crack propagation path (Inside the red line is the weld areacurves of precracked the NZ).

3.2. Crack Propagation Rate

Figure 5 shows the curves of the crack propagation rate of the precracked SMA490BW welded joint on the NZ and HAZ. The crack propagation rate of the NZ sample was different from that of the HAZ sample. With the increasing crack length, the crack propagation rate da/dN varied from 1×10^{-5} to 1×10^{-2} mm/cycle. During the whole process of crack propagation, the crack propagation rate of the NZ sample was slightly higher than that of the HAZ sample, because the performance of the NZ zone at the welded joint of SMA490BW after welding was weaker than that of the HAZ zone, which promoted the forward movement of crack propagation. The crack propagation length of the NZ and HAZ samples was also different at the time of failure, and the crack of the HAZ sample was significantly longer than that of the NZ sample. This could also explain the abovementioned phenomenon, as in the transient fracture region, the HAZ sample was deflected at the position with a longer crack length compared with the NZ sample.

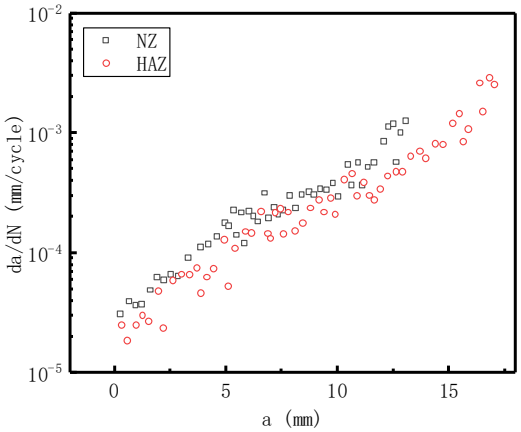

Figure 5. Multi-region crack growth rate comparison curve of SMA490BW welded joint.

Figure 6a,b show the comparison curves of the crack propagation rate of precracked SMA490BW welded joints in the NZ and HAZ zones between simulation and test samples. As shown in Figure 6a, it was found that the simulation results are basically consistent with the test results for the precrack and stable crack propagation stages of the NZ sample. In the late stage of stable propagation and the stage of unstable propagation, the simulation results are the above test results, which is related to the fluctuation of the crack propagation path when entering the stage of crack propagation and unstable propagation, as previously mentioned. It was also found that the length of the predicted crack rupture was longer than that measured in the experiment. As shown in Figure 6b, the simulation results of

HAZ samples are basically consistent with the test results for the precrack phase and the stable crack phase of crack expansion, but the agreement with the NZ samples is still poor. HAZ samples are heat-affected zones, and the mechanical properties of materials are not uniform. In the late stage of stable propagation and the unstable propagation stage, the simulation results are superior to the test results. Compared with the results of the NZ sample, it was found that the crack propagation rate of the HAZ sample fluctuated greatly. It was also observed, as mentioned above, that compared with the crack propagation path of the NZ sample, the HAZ sample was not as smooth. However, the predicted minimum crack propagation rate and maximum crack propagation rate are basically consistent with the experimental results. Here, the crack propagation rate curves obtained from the cosimulation are consistent with the test results, with an error of about 5%. The feasibility of joint simulation for crack propagation in different zones of the SMA490BW welded joint was verified.

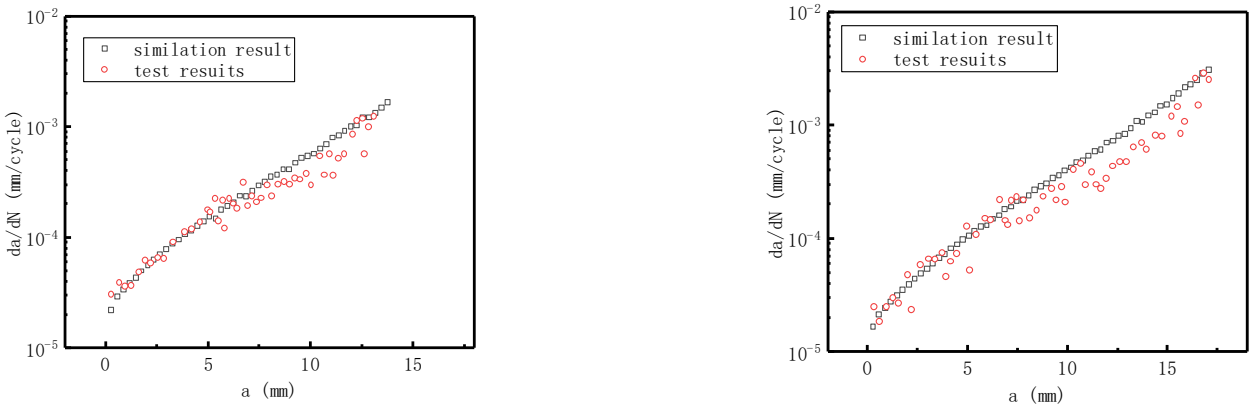

(**a**) NZ sample (**b**) HAZ sample

Figure 6. Multi-region crack propagation rate curve of SMA490BW welded joint.

3.3. Life Prediction

Figure 7 shows the *a*–*N* curves of precracked the NZ and HAZ samples. When loading 5000 cycles, the crack lengths of the NZ and HAZ samples showed little difference. With an increase in loading times, the crack gap between the NZ and HAZ samples continued to increase, and the crack propagation of the HAZ sample was accelerated. When the loading cycle reached 86,000 cycles, the crack length of the NZ specimen was 5.73 mm; then, the crack propagation period of the NZ specimen reached 4/5 of the sample lifetime and that of the HAZ specimen was about 1/2 of the sample lifetime. With an increase in the loading cycle, the crack propagation of the NZ specimen occurred when the loading cycle reached 107,800 cycles, while that of the HAZ specimen entered the stage of medium-to-high-speed expansion. When the loading cycle reached 165,300 cycles, the HAZ sample broke. At fracture, the crack length of the NZ sample was 13 mm, and its corresponding lifetime was 107,800 cycles. The crack length of the HAZ sample was 17 mm, and its corresponding lifetime was 165,300. The lifetime of the HAZ sample was 1.5 times that of the NZ sample. The reason for the difference in their crack propagation life is that the strength of the HAZ of the welded SMA490BW joint was higher than that of the NZ, which hinders the crack propagation to a certain extent, making the crack propagation life of the HAZ sample longer than that of the NZ sample. At the same time, the crack length at the time of fracture also indicates that the HAZ sample had a smaller transient fault zone than the NZ sample, and its structure was more stable than that of the NZ sample.

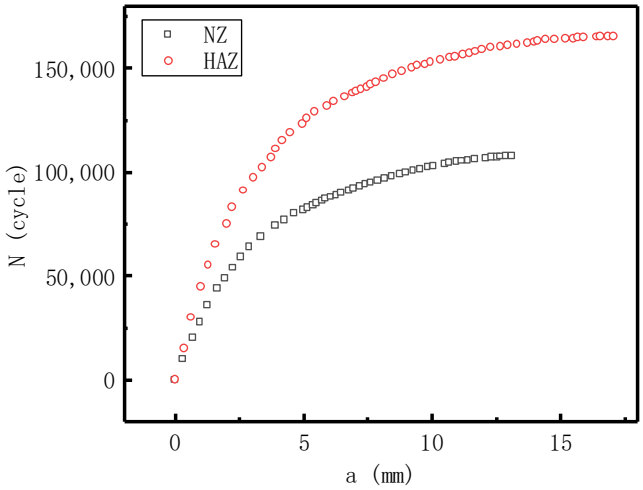

Figure 7. Multi-region crack growth life comparison curve of SMA490BW welded joint.

After obtaining the stress intensity factor at the crack tip at each analysis step using FRANC 3D, life prediction can be made using the Paris formula, which is expressed as follows:

$$\frac{da}{dN} = C(\Delta K)^m = \int_{a_0}^{a_p} \frac{da}{C(\Delta K)^m}$$

where ΔK is the amplitude value of the stress intensity factor and a_0 is the initial crack length. Figure 8 shows the a–N comparison curve drawn with the test and simulation results. As shown in Figure 8a, the simulation result of the NZ specimen is always superior to the test result, but its crack propagation life at fracture was basically consistent with the test result. As shown in Figure 8b, the simulation results of HAZ samples are in good agreement with the test results, and the simulation results fluctuate up and down with the test results. At fracture, the predicted lifetime of the NZ sample was 112,609 cycles, and the lifetime observed in the test was 107,800 cycles. At fracture, the predicted lifetime of the HAZ sample was 159,345 cycles, and the lifetime observed in the test was 165,300 cycles. The relative error between the test life span and the predicted life span of the FRANC 3D simulation was within 5%, indicating that cosimulation based on ABAQUS and FRANC 3D is a feasible method for predicting fatigue crack propagation life.

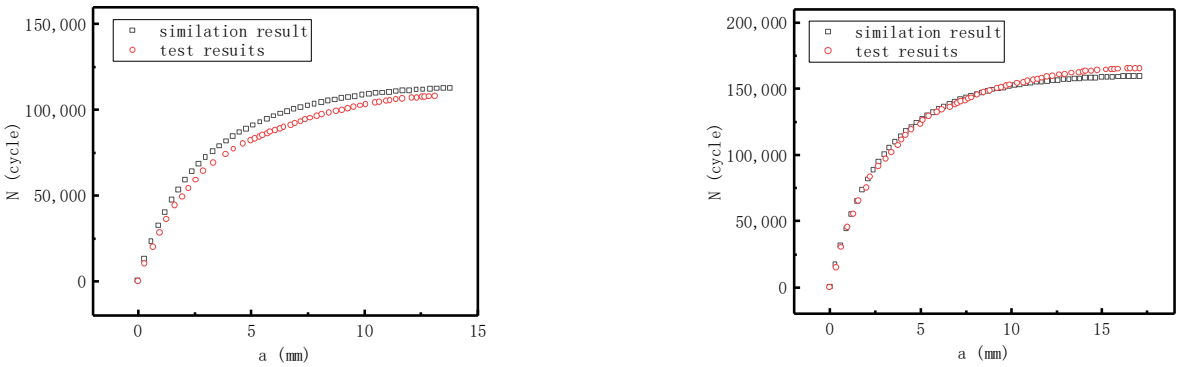

(**a**) NZ sample (**b**) HAZ sample.

Figure 8. Multi-region crack propagation life of SMA490BW welded joint.

3.4. Analysis and Discussion

Under the same stress level, the microscopic fractures of the two samples in the crack propagation stage and the transient fracture zone were compared. Fatigue striations and secondary cracks mainly characterized the microstructure morphology of the expanding

stage, while dimples mainly characterized the transient fracture area. Under cyclic loading, the crack tip was constantly opened and passivated, extending and sharpening, thereby leaving traces at the fracture point, called fatigue speckles; moreover, the direction of fatigue speckles was perpendicular to the direction of crack propagation. As shown in Figures 9a and 10a, numerous fatigue striations, fracture steps, and river morphologies [22,23] were present in the fracture points of NZ and HAZ samples. On comparing the two specimens, the crack propagation rate of the NZ specimen was higher than that of the HAZ specimen due to the larger spacing between the cracks. As shown in Figure 5, the crack growth rate of the NZ specimen was always above that of the HAZ specimen. Furthermore, secondary cracks were observed during the crack propagation, whose direction was perpendicular to that of the crack propagation. Additionally, this would consume part of the energy in the process of crack propagation and hinder the crack propagation. As shown in Figure 6, the crack propagation rate of the NZ and HAZ samples obtained through simulation in the late stage of stable propagation was higher than that measured in the test, because it is difficult to calculate the effect of secondary cracks on the crack propagation rate using FRANC 3D. Figures 9b and 10b show the morphologies of the transient fault zone of the NZ and HAZ samples. Both samples were observed to have ductile fractures, and the dimples in the transient fault zone of the HAZ sample were smaller and denser than those in the NZ sample. Therefore, the fatigue crack propagation test showed that the life span of the HAZ specimen with precracks was higher than that of the NZ specimen.

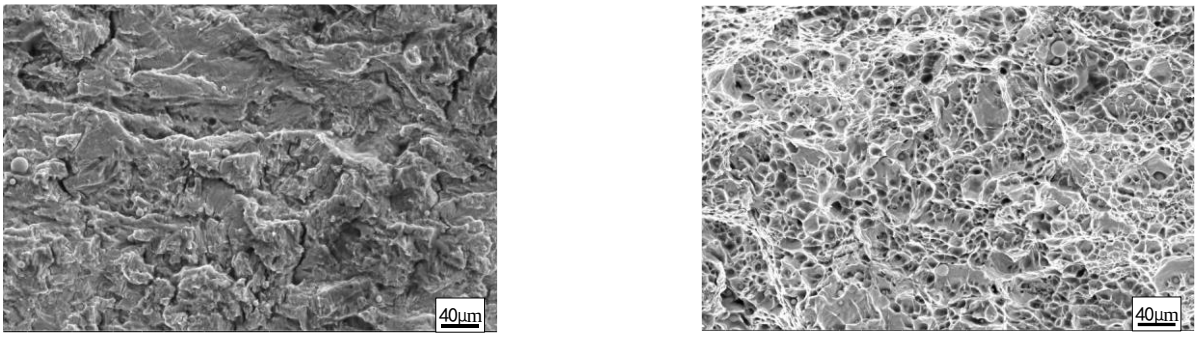

(**a**) extended area (**b**) Transient fault area

Figure 9. Microscopic fracture morphologies of NZ sample crack propagation.

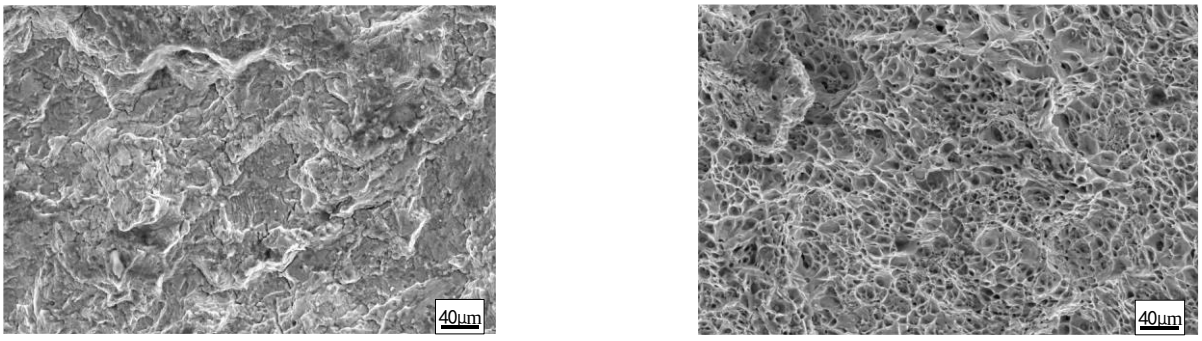

(**a**) extended area (**b**) Transient fault area

Figure 10. Microscopic fracture morphologies of HAZ sample crack propagation.

4. Conclusions

(1) The initiation, propagation, and transient fracture processes of the NZ and HAZ samples of the SMA490BW welded joint were all in the weld zone. The cracks extended along a straight line, and only a small angle of deflection appeared in the transient fracture zone.

(2) In the stable expansion stage of the SMA490BW welded joint, the crack propagation rate of the NZ sample was higher than that of the HAZ sample because the performance of the NZ was weaker than that of the HAZ.
(3) The crack propagation behavior of the SMA490BW welded joint was analyzed using the FRANC 3D and ABAQUS cosimulation method. The crack propagation path and crack propagation rate of the NZ and HAZ samples were consistent with the test results, thereby verifying the feasibility of the cosimulation.
(4) The test results show that the life span of the HAZ sample was higher than that of the NZ sample. Moreover, the relative error between the two sample's crack propagation prediction and test results using the FRANC 3D was about 5%, which verifies that the FRANC 3D is accurate in predicting the crack propagation life of the SMA490BW welded joint.

Author Contributions: Conceptualization, L.X.; Methodology, S.Z.; Software, D.L.; Investigation, J.A.; Writing—original draft, X.X.; Project administration, Y.H. All authors have read and agreed to the published version of the manuscript.

Funding: The APC was funded by the National Natural Science Foundation of China (no. 52105157) and the China Postdoctoral Science Foundation (2023MD734242).

Conflicts of Interest: The authors declare no conflict of interest.

Nomenclature

a	crack length
da/dN	fatigue crack growth rate
E	elasticity modulus
F	loading load
N	number of cycles
R	stress ratio
μ	Poisson ratio
σ_s	yield strength
ΔK_{th}	threshold value
ΔK	stress intensity factor range

References

1. Wu, Y.S.; Zhang, Z.Y.; He, Y.P.; Hui, C.; Yuanxing, L. Study on Microstructure and Mechanical Properties of SMA490BW Weathering Steel Welded Joints at Low Temperature. *Hot Work. Technol.* **2016**, *45*, 51–54. (In Chinese)
2. Seo, J.W.; Hur, H.M.; Jun, H.K.; Kwon, S.J.; Lee, D.H. Fatigue Design Evaluation of Railway Bogie with Full-Scale Fatigue Test. *Adv. Mater. Sci. Eng.* **2017**, *2017*, 5656497. [CrossRef]
3. Sun, Z.W.; Wu, X.Y.; Zhang, Z.Y.; He, Y.P.; Li, Y.X.; Chen, H. Study on Microstructures and Mechanical Properties of SMA490BW Steel Double Wire Welded Joints. *Hot Work. Technol.* **2016**, *45*, 55–58. (In Chinese)
4. Wu, X.Y.; Qi, W.C.; Liu, Y.J.; Han, Y.B.; Xia, C.H. Effect of Different Methods on Properties of SMA490BW Steel Welded Joints. *Adv. Mater. Res.* **2015**, *1095*, 902–905. [CrossRef]
5. Xu, L.; Su, J.J.; Zhou, S.; Hui, L. Study on Fatigue Properties of SMA490BW Steel for Bogie. *Hot Work. Technol.* **2020**, *49*, 30–34. (In Chinese)
6. He, B.; Deng, H.; Jiang, M.; Wei, K.; Li, L. Effect of ultrasonic impact treatment on the ultra high cycle fatigue properties of SMA490BW steel welded joints. *Int. J. Adv. Manuf. Technol.* **2018**, *96*, 1571–1577. [CrossRef]
7. Wu, X.; Zhang, Z.; Qi, W.; Tian, R.; Huang, S.; Shi, C. Corrosion Behavior of SMA490BW Steel and Welded Joints for High-Speed Trains in Atmospheric Environments. *Materials* **2019**, *12*, 3043. [CrossRef] [PubMed]
8. Zhang, X.; Dong, Y.; Lv, Q.; Gou, G.; Gao, W. Influence of humidity on crack propagation in the welding joint. *Int. J. Mod. Phys. B* **2020**, *34*, 2040055. [CrossRef]
9. Song, W.; Man, Z.; Xu, J.; Wang, X.; Liu, C.; Zhou, G.; Berto, F. Fatigue crack growth analysis of weathering steel joints based on analytical algorithm and J-integral method. *Trans. China Weld. Inst.* **2022**, *43*, 17–23+114. (In Chinese)
10. *BS7910*; Guide to Methods for Assessing the Acceptability of Flaws in Metallic Structures. British Standards Institution (BSI): London, UK, 2019.
11. Xiong, X.; Yang, Y.; Wang, Z.; Gan, J.; Wang, X.; Gai, W.; Li, Y. Fatigue crack growth analysis and life prediction based on FRANC3D and ABAQUS co-simulation. *J. Wuhan Univ. Technol.* **2020**, *44*, 506–512. (In Chinese)

12. Liao, Y.; Li, Y.; Pan, Q.; Huang, M.; Zhou, C. Residual fatigue life analysis and comparison of an aluminum lithium alloy structural repair for aviation applications. *Eng. Fract. Mech.* **2018**, *194*, 262–280. [CrossRef]
13. Park, C.Y.; Grandt, A.F.; Suh, J.J. Stress intensity factors for surface cracks at countersunk holes. *Eng. Fract. Mech.* **2006**, *73*, 1878–1898. [CrossRef]
14. Giannella, V.; Sepe, R.; Borrelli, A.; De Michele, G.; Armentani, E. Numerical investigation on the fracture failure of a railway axle. *Eng. Fail. Anal.* **2021**, *129*, 105680. [CrossRef]
15. Giannella, V. Stochastic approach to fatigue crack-growth simulation for a railway axle under input data variability. *Int. J. Fatigue* **2021**, *144*, 106044. [CrossRef]
16. Wang, L.; Zeng, H.; Liu, X.; Hui, L.; Cong, J. Effect of grinding methods on fatigue properties of SMA490BW weathering steel cross welded joints. *Weld. Join.* **2021**, *582*, 12–16+63–64.
17. *GB/T2975*; Steel and Steel Products—Location and Preparation of Samples and Test Pieces for Mechanical Testing. State Administration for Market Regulation: Beijing, China, 2018.
18. GB/T228.1*Metallic Materials—Tensile Testing—Part 1: Method of Test at Room Temperature*; State Administration for Market Regulation: Beijing, China, 2010.
19. Paris, P.C.; Erdogan, F. A Critical Analysis of Crack Propagation Laws. *J. Basic Eng. ASME* **1963**, *84*, 528–534. [CrossRef]
20. Paris, P.C.; Gomez, M.P.; Anderson, W.P. A Rational Analytic Theory of Fatigue. *Trend Eng.* **1961**, *13*, 9–14.
21. *GB/T6398*; Standard Test Method for Fatigue Crack Growth Rates of Metallic Materials. State Administration for Market Regulation: Beijing, China, 2000.
22. Huang, B.; Wang, L.; Hui, L.; Cong, J.; Zhou, S. Analysis of Multi-zone Fatigue Crack Growth Behavior of Friction Stir Welded 5083 Aluminum Alloy. *J. Mater. Eng. Perform.* **2022**, *31*, 53–63. [CrossRef]
23. Peng, Z.; Yang, S.; Wang, Z.; Gao, Z. Fatigue Property and Small Crack Propagation Mechanism of MIG Welding Joint of 6005A-T6 Aluminum Alloy. *Materials* **2022**, *15*, 4698. [CrossRef] [PubMed]